Machine Learning-Enabled LOS/NLOS Identification for MIMO System in Dynamic Environment

Chen Huang, *Student Member, IEEE,* Andreas F. Molisch, *Fellow, IEEE,* Ruisi He, *Senior Member, IEEE,* Rui Wang, *Student Member, IEEE,* Pan Tang, *Student Member, IEEE,* Bo Ai, *Senior Member, IEEE,* Zhangdui Zhong, *Senior Member, IEEE*

***Abstract*—Discriminating between line-of-sight (LOS) and non-line-of-sight (NLOS) conditions, or *LOS identification*, is important for a variety of purposes in wireless systems, including localization and channel modeling. LOS identification is especially challenging in vehicle-to-vehicle (V2V) networks since a variety of physical effects that occur at different spatial/temporal scales can affect the presence of LOS. This paper investigates machine learning techniques for LOS identification in V2V networks using an extensive set of measurement data and then develops robust and efficient identification solutions. Our approach exploits several static and time-varying features of the channel impulse response (CIR), which are shown to be effective. Specifically, we develop a fast identification solution that can be trained by using the power angular spectrum. Moreover, based on the measurement data, we also compare three different machine learning methods, i.e., support vector machine, random forest, and artificial neural network, in terms of their ability to train and generate the classifier. The results of our experiments conducted under various V2V environments, which were then validated using K-fold cross-validation, show that our techniques can distinguish the LOS/NLOS conditions with an error rate as low as 1%. In addition, we investigate the impact of different training and validating strategies on the identification accuracy.**

***Index Terms*—Line-of-sight identification, machine learning, device-to-device connections, localization, channel modeling**

Part of the work was presented at the IEEE ICC 2019 [25]. This work was supported in part by the National Natural Science Foundation of China under Grant 61922012, 61771037, 61961130391, U1834210, the National Key R&D Program of China under Grant 2018YFF0212103 and 2016YFE0200900, the Beijing Natural Science Foundation under Grant 4182047, the State Key Laboratory of Rail Traffic Control and Safety under Grant RCS2020ZT008, the Fundamental research funds for the central universities under Grant 2017RC031, the Royal Society Newton Advanced Fellowship under Grant NA191006. The work of Andreas F. Molisch and Rui Wang was supported by the California Transportation Authority under the METRANS project 14-11 and the National Science Foundation under NSF ECCS-1731. During part of this work, C. Huang, R. Wang, and P. Tang were with the University of Southern California, Los Angeles, USA. (*Corresponding author: Ruisi He and Bo Ai*.)

Chen Huang is with the School of Computer and Information Technology, Beijing Jiaotong University, Beijing, 100044, China (email: morning@bjtu.edu.cn).

Andreas F. Molisch is with the Ming Hsieh Department of Electrical and Computer Engineering, University of Southern California, Los Angeles, CA 90089 (email: molisch@usc.edu).

Ruisi He, Bo Ai, and Zhangdui Zhong are with the State Key Laboratory of Rail Traffic Control and Safety, Beijing Jiaotong University, Beijing 100044, China (email: ruisi.he@bjtu.edu.cn; boai@bjtu.edu.cn; zhdzhong@bjtu.edu.cn).

Rui Wang is with Samsung Research America, Mountain View, California, CA 94043 (email: rui1.w@samsung.com).

Pan Tang is with the State Key Lab of Networking and Switching Technology, Beijing University of Posts and Telecommunications, Beijing, 100876, China (email: tangpan27@bupt.edu.cn).

I. Introduction

DIFFERENTIATING line-of-sight (LOS) from non-line-of-sight (NLOS) channels (henceforth simply called LOS identification) based on real-time measured radio characteristics is important for a variety of applications in wireless systems, such as localization [1], [2] and channel modeling. Many localization systems, such as the Global Positioning System (GPS) and Cellular 911 Localization, are based on the measurements of the runtime between anchor nodes with known location and the agent node whose location has to be determined. However, there may be obstacles within the environment that can block the LOS connection between the nodes (i.e., NLOS situation), thereby introducing a (positive) bias in the distance estimation [3], [4]. Distinguishing such channels from LOS channels based on easily measurable quantities is important to enable developers to either discard NLOS runtime measurements or reduce their harmful effects through advanced signal processing [5], [6]. Another important application of LOS identification is channel modeling since most channel models [7], e.g., 3GPP [8], COST 2100 [9], use different channel parameters in LOS and NLOS situations.

LOS identification is especially difficult in device-to-device connections [10] such as vehicle-to-vehicle (V2V) communications [11]. V2V propagation channels are typically time-varying, nonstationary, and show different characteristics under LOS/NLOS conditions [12]–[14]. Due to the mobility of vehicles and due to the rich-scattering environment, other vehicles or buildings along the street may randomly block or reflect on the wireless signals. This makes it difficult to predict the LOS/NLOS condition based only on the type of environment. Furthermore, the propagation channel characteristics usually evolve as the vehicles with the transmitter (Tx) and receiver (Rx) move.

LOS identification is very important, thus, several solutions have been proposed:

1) *Conducting visual inspection by cross-checking video data and measurement data:* In some environments, the LOS and NLOS conditions occur randomly when cars or pedestrians block the signal. For example, [15] used a recording from cameras mounted near the Tx and Rx to distinguish the LOS and NLOS situations.
2) *Designing measurement campaign to distinguish the scenarios inherently:* The most direct way of channel

modeling is to individually measure the channels in the LOS and NLOS scenarios. For example, [16] measured the V2V channel in an intersection scenario, in which the Tx and Rx cars first move in convoy and then move in different directions at the intersection. Thus, the measurement campaign inherently separates the LOS and NLOS environments.

3) *Using some characteristic parameters of the propagation channel to determine whether it is a LOS or NLOS scenario:* For example, [17] used the Rician K-factor to estimate whether it is a LOS or an NLOS scenario.

Despite the different solutions offered by these LOS identification techniques, there are still drawbacks to the current solutions:

1) Although a visual inspection can perform LOS identification accurately, the process is time-consuming and exhausting for human observers.
2) Designing the measurement campaigns to inherently provide LOS or NLOS is difficult because the surrounding nonstatic objects, e.g., cars, might change the LOS state; this may happen in an unpredictable manner.
3) Solutions that are based on deterministic thresholds of channel parameters are usually not accurate enough in time-varying channels.

Meanwhile, machine learning tools are well suited for addressing classification problems. As such, applying machine learning-based techniques to the identification of LOS/NLOS conditions more promises to provide more accurate results since ML methods can extract the pattern from multiple dimensions of channel features. Thus, various such methods have been investigated in the literature. Ref. [18] uses a support vector machine (SVM) to identify the LOS/NLOS scenarios, where the received power, maximum power, rise time, kurtosis, and delay spread are extracted as the training features. Similarly, [19], [20] train the SVM by using the channel features mentioned above with the addition of skewness and the fitness between the measurement data and Rician distribution. Instead of using SVM, [21] develops an NLOS identification algorithm by conducting a relevance vector machine (RVM) with similar training features [18]. Compared to the SVM, the RVM usually requires a longer training time but can be evaluated faster in actual implementation. Recently, [22] exploits random forest (RF) for LOS/NLOS classification, where the channel impose responses (CIRs) are adopted as training features. Moreover, as a well known machine learning method, the artificial neural network (ANN) has been adopted in [23] and trained by using typical channel features, e.g., Rician K-factor and kurtosis, to identify the LOS/NLOS channels, whereas [24] trains the ANN by using de-noised channel state information (CSI).

Although a variety of channel quantities related to the SISO (single-input-single-output) impulse response have been exploited in the past for LOS identification (both for deterministic threshold methods and for machine learning), the antenna arrays present in most modern wireless transceivers enable researchers to also observe the angular channel information. However, none of these above methods clearly address the LOS identification problem by exploiting the angular information in channels. The angular properties of the channels are closely related to the geometry of the environment; thus, these properties are likewise strongly associated with LOS/NLOS conditions. Moreover, the time-varying channels, which are usually considered in dynamic environments, are expected to consist of the dynamic characteristics that may help to improve the LOS identifications. Inspired by this, we propose in this paper an angular information-based LOS identification method for time-varying channels.

In our conference paper [25], we briefly introduced the idea of using the static angular information to identify LOS/NLOS in multiple-input multiple-output (MIMO) systems. In this paper, we extend this and propose a time-varying angular information-based LOS identification solution. We also evaluate how the following factors would affect the accuracy of LOS/NLOS identification: i)*machine learning methods for training*, ii) *training features*, and iii) *training and validating strategies*. Through the experiments based on the channel measurement data, it is found that the proposed time-varying angular feature can significantly improve both the NLOS identification accuracy and the robustness in different scenarios compared with the current studies, e.g., [23], [24]. Accordingly, the main contributions of this paper are as follows:

- We use the time-varying angular properties of channels to develop an intelligent LOS identification algorithm that can improve identification accuracy. In particular, we propose a LOS identification solution that uses the power angular spectrum (PAS) as the identification object instead of the directional features of the multipath components (MPCs) as extracted by high-resolution parameter estimation (HRPE). Apparently, this will make the localization applications and the data processing for channels research more accurate;
- We investigate the feasibility of using various features of the collected V2V measurement data for LOS identification; some of them have been shown to be effective in the past. We demonstrate that using a single feature does not give sufficient identification accuracy; hence, we propose to apply machine learning to exploit multiple channel features simultaneously.
- We investigate several machine learning methods for the LOS identification. We evaluate the identification performance of SVM, RF, and ANN based on extensive V2V measurement data. These methods show different performances when different training features and training strategies are used.
- Compared with the widely used K-fold cross-validation, we use more practical training strategies to evaluate all the identification solutions. The training and testing data are collected from: i) *different streets* and ii) *different parts of each street*. The former approach may be less accurate to use; however, it might be more practical and easier to implement.

The remainder of the paper is organized as follows. Section II formulates the problem and introduces the framework of the proposed approaches. Section III presents the feature

extraction schemes. Section IV presents three methods that can be used to train the LOS/NLOS classifier. We present the V2V measurement campaign in section V and evaluate the proposed algorithm under various settings in section VI. Lastly, we conclude our findings in section VII.

II. Problem Description

We aim to determine whether LOS (defined as an "optical" LOS between Tx and Rx) is present in the measured channel characteristics. As the TX and Rx move, the LOS might change with time as well.

We consider a wireless transmission system that can be used for communications or localizations, or both. In any case, the system transmits a known training signal (pilot signal, reference signal) with Fourier transform $\mathbf{X}(f)$; the frequency-domain representation of the received signal is written as $\mathbf{Y}(f)$. Both $\mathbf{X}$ and $\mathbf{Y}$ are vectors of functions, representing the signals transmitted to/received from the different antenna array elements at the Tx and Rx, respectively. The channel is thus represented by a matrix transfer function (TF), $\mathbf{H}(f)$; its elements are the TFs between the various Tx and Rx antenna elements. This TF matrix is related to parameters of the multipath components (MPCs) [27]:

$$\mathbf{H}(f) = \sum_{l=1}^{L} \alpha_l \cdot \mathbf{c}_2(\Omega_{2,l}) \cdot \mathbf{c}_1(\Omega_{1,l})^T \cdot e^{-j2\pi f \tau_l}, \qquad (1)$$

where L is the total number of multipath components (MPCs); $\delta(\cdot)$ is the Dirac delta function; and α_l, τ_l denote the complex amplitude and delay, respectively, associated with the lth MPC. The vectors $\mathbf{c_2}(\Omega_{2,l})$, $\mathbf{c}_1(\Omega_{1,l})$ are the steering vectors on the Rx and Tx sides, respectively, whereas the expression $\Omega_{i,l} = [\cos(\phi_{i,l})\sin(\theta_{i,l}), \sin(\phi_{i,l})\sin(\theta_{i,l}), \cos(\theta_{i,l})]$, $i = 1, 2$ determine directions/angles in a spherical coordinate system. The term$(\phi_{i,l}, \theta_{i,l}) \in [-\pi, \pi) \times [0, \pi]$. $\phi_{2,l}, \theta_{2,l}, \phi_{1,l}, \theta_{1,l}$ is the azimuth of arrival (AOA), elevation of arrival, azimuth of departure (AOD), and elevation of departure of the lth path, respectively. Lastly, $(\cdot)^T$ is the transposition operation. From Eq. (1), we can extract various channel parameters, including power, delay, and the angle of the MPCs.[1] Note that the directly observable quantities are (vector) impulse responses/TFs, while obtaining the MPC parameters requires sophisticated and computationally expensive HRPE.

Various channel parameters can help researchers to discriminate between LOS/NLOS conditions. A large number of measurements have shown that the LOS and NLOS data have different distributions of received power as function of delay, an example of which is shown in Fig. 1. Although we can see an obvious difference in the power delay profiles (PDPs), it is hard to assign a simple quantitative rule that can determine whether a LOS is present. Since Tx and Rx are moving, we may consider a sequence of $T(T \geq 1)$ temporal snapshots, denoted by $[\mathbf{h}^{(1)}, \mathbf{h}^{(2)}, \cdots, \mathbf{h}^{(T)}]$. This may provide additional information, and thus make the LOS identification more accurate.

[1] Note that the elevation domain may not be considered in some cases, e.g., the data are collected by a horizontal uniform linear array.

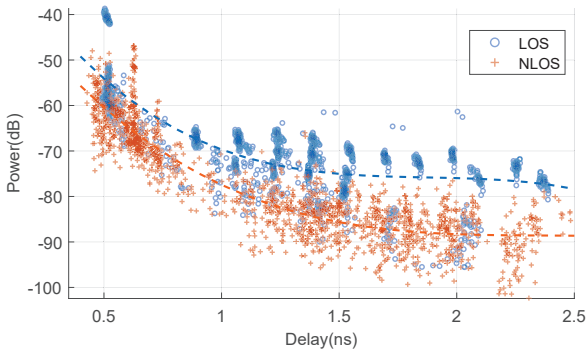

Fig. 1. Example LOS and NLOS power delay profile data from the measurement campaign described in Sec. V.

This work investigates how the channel features derived from the MPC parameters (discussed further in section III) impact the LOS identification. However, we do not focus only on the impact of the MPC parameters; we also seek to compare such impact to the fast estimation result, e.g., PAS, directly obtained from the channel measurements (e.g., via Bartlett beamforming).

Therefore, the main problems are: 1) how can we identify the LOS and NLOS scenarios accurately based on the propagation channel features and 2) which channel features contribute most to the LOS identification.

The proposed framework has two major stages: training and testing. The training stage consists of the following steps:

1) We perform an extensive V2V measurement campaign to collect training data; the details of the measurement campaign are presented in section V. Accordingly, we can obtain the CIR over time $[h^{(1)}, h^{(2)}, \cdots, h^{(T)}]$. Ground truth labeling (LOS/NLOS) is obtained for each location by visual inspection.
2) We then extract the channel features from the collected data and use them as the training data $\mathbf{X} = [\mathbf{x}^{(1)}, \mathbf{x}^{(2)}, \cdots, \mathbf{x}^{(T)}]$. These are then further divided into two categories: high-resolution estimation results $\mathbf{X}^{\mathrm{h}}$ and low-resolution estimation results $\mathbf{X}^{\mathrm{l}}$.
3) We generate the classifiers by using SVM, RF, and ANN, respectively, based on the training data.
4) Lastly, we test and evaluate all the classifiers by using different training and testing strategies. Specifically, we use three different training and testing strategies to do an actual evaluation of the algorithm. The details of the evaluation are presented in section VI.

The general system architecture of this paper is shown in Fig. 2.

III. Feature Extraction

This section presents the process of identifying the key features of the collected CIRs and their use in identifying the LOS/NLOS conditions. Specifically, the extracted features fall under two categories: high-resolution estimation parameters and low-resolution estimation results. In the former case, we extract the channel parameters of the MPCs by using HRPE algorithms such as the space-alternating generalized

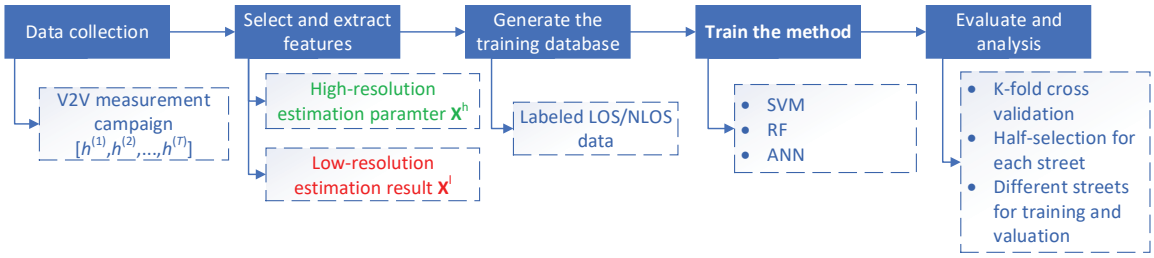

Fig. 2. System architecture of the proposed LOS/NLOS identification technique.

expectation-maximization (SAGE) [28] or joint maximum likelihood estimation (RiMax) [29]. We will then apply the latter to the results in Section V.

A. Channel Property Characterization

We extract from the measured (or simulated) propagation channels those features that are expected to capture the salient differences between the LOS and NLOS conditions for each snapshot:

Maximum received power over delay samples ($\max(|h^{(t)}|^2)$): The LOS MPC generally contains more power than the NLOS MPC. Therefore, the maximum received power of each snapshot $\max(|h^{(t)}|^2)$ can be used to identify LOS situations..

Kurtosis of the received power ($\mathcal{K}^{(t)}$): This can measure the peakedness of the amplitude probability distribution and is defined as the ratio between the fourth- and the second-order moments of the received signal's amplitude:

$$\mathcal{K}^{(t)} = \frac{\mathrm{E}[(|h^{(t)}| - \mu_{|h^{(t)}|})^4]}{\mathrm{E}[(|h^{(t)}| - \mu_{|h^{(t)}|})^2]^2} = \frac{\mathrm{E}[(|h^{(t)}| - \mu_{|h^{(t)}|})^4]}{\sigma^4_{|h^{(t)}|}} \quad (2)$$

where $\mu_{|h^{(t)}|}$ and $\sigma_{|h^{(t)}|}$ are the mean and standard deviation of $|h^{(t)}|$. Accordingly, this can be expressed as:

$$\mu_{|h^{(t)}|} = \frac{\sum_{l=1}^{L} ||h(t_l)| - |\bar{h}(t)||}{L} \quad (3)$$

$$\sigma_{|h^{(t)}|} = \sqrt{\frac{\sum_{l=1}^{L} (|h(t_l)| - |\bar{h}(t)|)^2}{L}}. \quad (4)$$

The amplitude of signals in the NLOS scenario are usually less peaked than that in the LOS scenario; thus, the kurtosis is generally larger in LOS conditions.

Skewness of the received power ($\mathcal{S}^{(t)}$): This can be used to measure the asymmetry of the probability distribution. The skewness of a Rayleigh distribution is generally larger than that of a Rician distribution; in other words, the NLOS data are usually more skewed than the LOS data. The skewness can be calculated as:

$$\mathcal{S}^{(t)} = \frac{\mathrm{E}(|h^{(t)}| - \mu_{|h^{(t)}|})^3}{\sigma^3_{|h^{(t)}|}} \quad (5)$$

where $\mu_{|h^{(t)}|}$ and $\sigma_{|h^{(t)}|}$ are given in (3) and (4), respectively.

Rising time ($\Delta\tau^{(t)}$): This measures the time interval between the strongest MPC and the first MPC:

$$\Delta\tau^{(t)} = \arg\max_{\tau} |h^{(t)}| - \min(\tau_l) \quad (6)$$

where l is the index of the MPCs. The first components in NLOS scenarios might be attenuated by blocking objects or strong diffractions; hence, the rising time in NLOS scenarios is usually larger than that in LOS scenarios.

Root mean square-delay spread ($\tau^{(t)}_{rms}$): This measures the root mean square (RMS) delay spread of all MPCs in the current snapshots:

$$\tau^{(t)}_{rms} = \sqrt{\frac{\sum_{l=1}^{L} (\tau_l^{(t)} - \tau_m^{(t)})^2 |h_l^{(t)})|^2}{\sum_{l=1}^{L} |h_l^{(t)}|^2}} \quad (7)$$

where $\tau_m^{(t)}$ is the mean excess delay. Accordingly, this can be expressed as:

$$\tau_m^{(t)} = \frac{\sum_{l=1}^{L} \tau_l |h_l^{(t)}|^2}{\sum_{l=1}^{L} |h_l^{(t)}|^2}. \quad (8)$$

The single strongest component (i.e., LOS) is absent in an NLOS channel, which tends to lead to a lower concentration of the power in delay. Hence, the RMS-delay spread is generally higher in NLOS than in LOS scenarios.

Rician *K*-factor ($K_{\mathrm{r}}^{(t)}$): The Rician K-factor is defined as the ratio between the power of a (possible) dominant MPC (typically the LOS) and the power in the remaining MPCs. Although a nonzero K-factor also exists in many NLOS situations, theoretical and empirical studies have shown that there is a correlation between the magnitude of the K-factor and the presence of LOS conditions. The K-factor can be roughly approximated as:

$$K_{\mathrm{r}}^{(t)} = \frac{(|h^{(t)}|_{\max})^2}{2\sigma^2_{|h^{(t)}|}} \quad (9)$$

where $|h^{(t)}|_{\max}$ represents the amplitude of the main peak in the tth snapshot and $\sigma_{|h^{(t)}|}$ is the variance of amplitude.

The features presented above are the indicators for LOS/NLOS identification that have been widely used in the literature. In this paper, we further study the static and temporal angular features to identify the NLOS/LOS scenarios more accurately.

Angular difference ($\Delta\lambda_l^{(t)}$): This measures the difference between the AOD (ϕ_1) and AOA (ϕ_2) of the strongest MPC in each snapshot. The strongest MPC in the LOS scenario should be the LOS MPC. In a LOS MPC, the signal transmitted from the Tx directly propagates to the Rx; thus, the angular difference between the AOD and AOA should remain constant (unless the cars turn at different times, or two oncoming cars

pass each other). On the other hand, the angular difference of an NLOS MPC may change instantly, e.g., due to dynamic reflectors in V2V channels or because the movement of Tx and Rx with respect to static reflectors changes the AOD and AOA. For the strongest MPC l in the tth snapshot, the angular difference is defined as:

$$\Delta\lambda_l^{(t)} = \left|\exp(i\phi_{1,l,max}^{(t)}) - \exp(i\phi_{2,l,max}^{(t)})\right|. \quad (10)$$

Angular spread of departure/arrival ($\lambda_{\mathrm{ASD}}^{(t)}/\lambda_{\mathrm{ASA}}^{(t)}$): This measures the spreads of AOA and AOD of all MPCs in the current snapshot. They can be calculated as [30]:

$$\lambda_{\mathrm{ASD/ASA}}^{(t)} = \sqrt{\frac{\sum_{l=1}^{L} |\exp(i\phi_{1/2,l}^{(t)}) - \mu_{\phi_{1/2}}^{(t)}|^2 |h_l^{(t)}|^2}{\sum_{l=1}^{L} |h_l^{(t)}|^2}} \quad (11)$$

where the $\mu_{\phi_{1/2}}^{(t)}$ is the mean direction of the PAS. This, in turn, can be calculated as:

$$\mu_{\phi_{1/2}}^{(t)} = \frac{\sum_{l=1}^{L} \exp(i\phi_{1/2,l}^{(t)}) |h_l^{(t)}|^2}{\sum_{l=1}^{L} |h_l^{(t)}|^2}. \quad (12)$$

The angle spread of LOS scenarios is generally smaller than that of NLOS scenarios.

Angular variant of departure/arrival ($\Delta\psi^{\phi_1,(t)}, \Delta\psi^{\phi_2,(t)}$): This measures the variation of the AOD and AOA of the strongest path at a certain time window. Assuming the time interval is Δt during the snapshots of $\{h^{(t-\Delta t)}, h^{(t-\Delta t-1)}, \cdots, h^{(t)}\}$, the AOD/AOA of the strongest path in each snapshot can be expressed as:

$$\mathbf{V}_{\phi_{1/2}}^{(t)} = [\phi_{1/2}^{(t-\Delta t)}, \phi_{1/2}^{(t-\Delta t-1)}, \cdots, \phi_{1/2}^{(t)}]^{\mathrm{T}} \quad (13)$$

which can be rewritten as:

$$\mathbf{V}_{\phi_{1/2}}^{(t)} = \begin{bmatrix} r\sin\phi_{1/2}^{(t-\Delta t)} & , & r\cos\phi_{1/2}^{(t-\Delta t)} \\ \vdots & & \vdots \\ r\sin\phi_{1/2}^{(t)} & , & r\cos\phi_{1/2}^{(t)} \end{bmatrix} = [\mathbf{v}_1, \mathbf{v}_2]. \quad (14)$$

In this case, we use the eigenvalue of the covariance matrix of the $\mathbf{V}_{\phi_{1/2}}$ to validate the dispersion of the AOA/AOD of the strongest path:

$$\Delta\psi^{\phi_{1/2},(t)} = \sum \mathrm{eig}\left(\begin{bmatrix} \mathrm{cov}(\mathbf{v}_1,\mathbf{v}_1) & \mathrm{cov}(\mathbf{v}_1,\mathbf{v}_2) \\ \mathrm{cov}(\mathbf{v}_2,\mathbf{v}_1) & \mathrm{cov}(\mathbf{v}_2,\mathbf{v}_2) \end{bmatrix}\right). \quad (15)$$

In summary, the input (feature) vector of the tth snapshot can be expressed as:

$$\mathbf{x}^{\mathrm{h},(t)} = \{\max(|h^{(t)}|^2), \mathcal{K}^{(t)}, \mathcal{S}^{(t)}, \Delta\tau^{(t)}, \tau_{\mathrm{rms}}^{(t)}, K_{\mathrm{r}}^{(t)}, \Delta\lambda_l^{(t)}, \lambda_{\mathrm{ASD}}^{(t)}, \lambda_{\mathrm{ASA}}^{(t)}, \Delta\psi^{\phi_1,(t)}, \Delta\psi^{\phi_2,(t)}\}. \quad (16)$$

Fig. 3 shows an example of kurtosis and the AOA obtained from our V2V channel measurements (see Section V). We can see from the figure that both these characteristics show different distributions in LOS and NLOS scenarios. However, there is no existing threshold that can be used to separate the LOS and NLOS data perfectly.

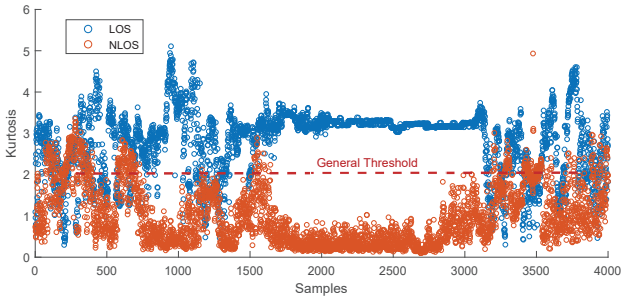

(a)

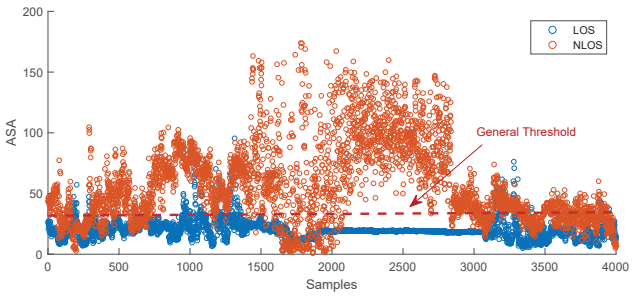

(b)

Fig. 3. Distribution of factors in LOS and NLOS, respectively. (a) Kurtosis (b) AOA

B. Power Angle Spectrum Extraction

Using the above angular features based on MPCs requires HRPE, which is computationally expensive. Instead, we can use the PAS as a low-resolution estimation training feature for comparison. The PAS cannot provide actual MPCs albeit it still contains angular information that can be used for further processing [31]. The PAS can be obtained by using the Bartlett beamformer [32], which is expressed as:

$$\mathbf{x}^{\mathrm{l},(t)}(\phi_1,\phi_2) = \frac{[\mathbf{c}_2(\Omega_{2,l}) \bigotimes \mathbf{c}_1(\Omega_{1,l})]^H \mathbf{R} [\mathbf{c}_2(\Omega_{2,l}) \bigotimes \mathbf{c}_1(\Omega_{1,l})]}{[\mathbf{c}_2(\Omega_{2,l}) \bigotimes \mathbf{c}_1(\Omega_{1,l})]^H [\mathbf{c}_2(\Omega_{2,l}) \bigotimes \mathbf{c}_1(\Omega_{1,l})]} \quad (17)$$

where the $(\bigotimes)$ denotes the Kronecker product and $\mathbf{R}$ is the spatial covariance matrix. The latter is defined as:

$$\mathbf{R} = \mathrm{E}\{\mathrm{vec}(\mathbf{H}(f))\mathrm{vec}(\mathbf{H}(f))^{\mathrm{H}}\} \quad (18)$$

where the $\mathrm{vec}(\cdot)$ operator stacks the columns of a matrix into a vector. The advantage of the PAS is that it is simple to implement; its drawback is its low resolution. Fig. 4 gives two examples of the estimated PAS in (a) LOS scenario and (b) NLOS scenario, respectively. The power distributions of the PASs in the LOS and NLOS scenarios obviously show different characteristics, and this can be used for identification.

IV. Machine Learning-Based LOS/NLOS Identification

We briefly present in this section the machine learning methods used to generate the LOS/NLOS classifier. Based on the set of features extracted from the CIRs, the task here is to decide whether a given set of CIR samples corresponds to LOS or NLOS conditions. We use three different generation

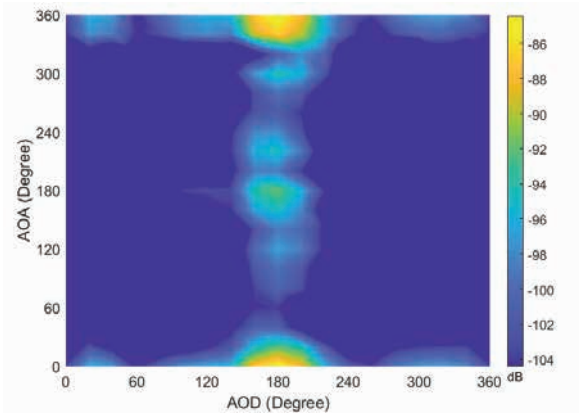

(a)

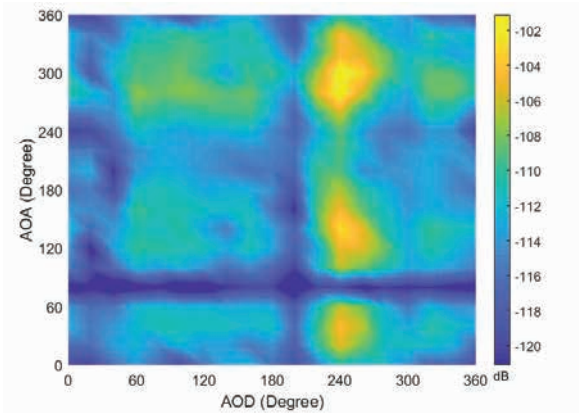

(b)

Fig. 4. Examples of the estimated PASs in the (a) LOS and (b) NLOS scenarios, respectively.

methods, namely, SVM, RF, and ANN; these methods are widely used to address various classification problems.

A. Least Square Support Vector Machine

The SVM is a supervised learning method that is mostly used for classification, especially for binary classification problems [33]. The SVM has been widely used for classification due to its robustness and because it requires only a few predefined parameters. Specifically, we use the least squares SVM (LS-SVM) [34], which uses an especially simple optimization to learn the weights in the SVM.

A linear classifier can be expressed as a function of $\mathbf{X} \Rightarrow \{-1, +1\}$ and has the following form:

$$\mathcal{L}^{(t)}(\mathbf{x}) = \text{sign}[w^T \varphi(\mathbf{x}^{(t)}) + w_0] \tag{19}$$

where the sign is the signum function and $\varphi(\mathbf{x})$ is the eigenvector of feature $\mathbf{x}$ after projection (described in more detail below). Meanwhile, w and w_0 are the weight parameters learned from the training data $\{\mathbf{x}^{(t)}, \mathcal{L}^{(t)}\}_{t=1}^{T}$, where $\mathbf{x}^{(t)} \in \mathbf{X}$ and the input labels $\mathcal{L}^{(t)} \in \{-1, +1\}$. In this case, the LS-SVM separates two classes $\{-1, +1\}$ by determining the separating hyperplane that maximizes the margin between the two classes. Therefore, we obtain the LS-SVM classifier by solving the following optimization problem:

$$\arg \min_{w, w_0, e, \sigma^2} \frac{1}{2}||w||^2 + c\frac{1}{2}\sum_{j=1}^{N}(e^{(t)})^2 \tag{20}$$

$$s.t. \quad \mathcal{L}^{(t)}[w^T \varphi(\mathbf{x}^{(t)}) + w_0] = 1 - e^{(t)}, \forall t \tag{21}$$

where c is the weighting factor that controls the trade-off between training error and model complexity. Fig. 3 shows that the LOS/NLOS scenario are not linearly separable. Considering this, we use a Gaussian radial basis function [35], instead of a linear mapping function, to classify the LOS/NLOS scenarios better:

$$k(\mathbf{x}, \mathbf{x}^{(t)}) = \varphi(\mathbf{x})^T \cdot \varphi(\mathbf{x}^{(t)}) = \exp\left[-\frac{||\mathbf{x} - \mathbf{x}^{(t)}||_2^2}{2\sigma^2}\right] \tag{22}$$

where σ^2 is the hyper-parameter learned from the training data using (20). The optimization problem (20) has already been established to be a linear programming problem [34]. This can be solved by using its Lagrangian dual and Karush-Kuhn-Tucker conditions in order to obtain the prediction of the LS-SVM as:

$$\mathcal{L}(\mathbf{x}) = \text{sign}\left[\sum_{t=1}^{T} \alpha^{(t)} \mathcal{L}_j k(\mathbf{x}, \mathbf{x}^{(t)}) + w_0\right] \tag{23}$$

where $\alpha^{(t)}$ is the Lagrange multiplier.

We then train an LS-SVM classifier to distinguish between LOS and NLOS scenarios using the input $\mathbf{x}^{(t)}$ and the corresponding labels $\mathcal{L}^{(t)} = -1$ and $+1$ for the NLOS and LOS data, respectively.

B. Random Forest

The RF is a kind of ensemble learning method [36] consisting of multiple different decision trees that use randomly selected features. The RF arrives at its final decision after all the decision trees have voted on the decision. In this case, the RF classifier usually has good robustness to overfitting. Likewise, it is widely accepted that RF provides a superior classification performance for a moderate complexity with relatively large feature size. Specifically, we use the classification and regression-RF (CART-RF) [37] in this study. Each decision tree in the CART-RF divides the input samples based on the Gini index of the input feature instead of the information entropy. Accordingly, this is defined as:

$$\text{Gini}(\mathbf{x}) = \sum_{\mathcal{L}=1}^{\mathcal{N}} p_{\mathcal{L}}(1 - p_{\mathcal{L}}) = 1 - \sum_{\mathcal{L}=1}^{\mathcal{N}} p_{\mathcal{L}}^2 \tag{24}$$

where $p_{\mathcal{L}}$ denotes the ratio of the samples $\mathbf{x}$ that have the label $\mathcal{L}$ and the total data $\mathbf{X}$, and $\mathcal{N}$ is the number of data categories. Each sample is either LOS or NLOS; thus, $\mathcal{N}$ is 2 in our case. The Gini index of a given feature x of the input data $\mathbf{X}$ is calculated as:

$$\text{Gini}(\mathbf{X}, x) = \frac{|\mathbf{X}^{x<x'}|}{|\mathbf{X}|}\text{Gini}(\mathbf{X}^{x<x'}) + \frac{|\mathbf{X}^{x>x'}|}{|\mathbf{X}|}\text{Gini}(\mathbf{X}^{x>x'}), \quad x \in \mathbf{x} \tag{25}$$

where x' is the threshold used to separate the data $\mathbf{X}$. We can obtain the optimal classification of feature x^* by minimizing the Gini index of x as follows:

$$x^* = \arg \min_{x \in \mathbf{x}, x'} \text{Gini}(\mathbf{X}, x). \tag{26}$$

C. Artificial Neural Network

ANN is an important and widely used machine learning tool, which was developed to solve classification, recognition, and regression problems [38]. A neural network is comprised of a number of basic elements called neurons, in which the input is transformed through linear mapping followed by a nonlinear activation. To train the network, we can apply a learning algorithm to the network in order to update the mapping parameters in the neurons until the output of the network is consistent with the target output. Specifically, we can train a neural network to learn a particular output by applying the learning process to a group of known samples with labels; we can then predict the output of the network using the validation samples. This is a widely investigated approach to learning a pattern that reveals a nonlinear relationship between the known input (measurement data) and target output (LOS or NLOS label). ANNs have good robustness in terms of learning ability and have a very flexible network design; thus, several studies have used ANNs for LOS/NLOS identification [23], [24].

In this paper, we adopt a neural network with feed-forward architecture and an error-back-propagation-based learning algorithm. This kind of neural network usually consists of an input layer, one or several hidden layers, and an output layer. The term "feed-forward" implies that the neural network has a topological structure in which only the links between two neighboring layers exist, i.e., the input layer can only be connected to the hidden layer while the hidden layer can be connected only to the output layer. It is noteworthy that, the conducted network structure can affect the performance of the identification: a complicated and highly custom network generally performs better but requires extensive experiments and adjustments, which is considered to be outside the scope of this paper. Consequently, we use a regular fullyconnected layer-based deep learning network in our experiments. In our case, we use the extracted channel features $\mathbf{X}^{\text{h},(t)}$ and the PAS $\mathbf{X}^{\text{l},(t)}$ as the input data, respectively. The activation function we use is:

$$f(x) = \begin{cases} x, & x \geq 0; \\ 0, & x < 0. \end{cases} \tag{27}$$

The parameters of the network, e.g., the number of hidden layers and the number of nodes in each layer, are crucial to the performance of the neural network, which is usually set empirically. In our case, we first select the approximate range of the network parameters based on the scale of input features and on the output labels; then, we further determine the actual parameters experimentally. Fig. 5 shows the final network architecture, in which five hidden layers with $\{128, 64, 32, 16, 8\}$ nodes are used. Note that the SoftMax function is conducted after the hidden layers such that the output of hidden layers can be mapped into the output label.

TABLE I
PARAMETERS AND SYSTEM SETUP OF THE MEASUREMENT CAMPAIGN

Parameter	Value
Carrier frequency	5.9 Ghz
Bandwidth	15 Mhz
Transmit power	26 dBm
Number of Tx antennas	8
Number of Rx antennas	8
Sampling rate	20 MS/s

V. MEASUREMENT CAMPAIGN

This section details the measurement campaign and parameter extraction procedure that we used in this study to generate the channel characteristics, and accordingly form the basis for the evaluation of our proposed algorithm. Likewise, this section discusses the data collection procedure for developing the different training and testing strategies (presented in section VI).

A. System Settings

We conducted the V2V measurement campaign using the self-built real-time MIMO channel sounder described in [39]. The sounder includes a pair of National Instrument-universal software radio peripheral (NI-USRP) reconfigurable input/output (RIO) devices that function as the main RF transceivers, two GPS-disciplined rubidium clocks that serve as the synchronization units, and a pair of eight-element uniform circular arrays that are connected to the USRPs via electronic switches. Table I provides the key parameters of the setup whereas Figs. 6(a) and (b) illustrate the measurement cars and antenna arrays used in this study.

We placed 360° cameras next to the Tx and Rx to record the environment during the whole measurement and accurately determine the "ground truth", i.e., whether LOS or NLOS is valid at a particular time. The data gathered are used for the training and for the performance assessment. Fig. 6(c) gives a sample snapshot of the video recorded from the Rx side. The details of the sounder and the measurement campaign can be found in [39], [40].

From the measured transfer function matrices, we extract, via RiMax, the parameters of the MPCs, which form the basis of most of the computations in Sec. VI. More detailed descriptions about the extraction methodology can be found in [40].

B. Route selection

We conducted the measurements on the campus of the University of Southern California, USA, and on public roads near the campus. The blue dots in Fig. 7 represent the positions of the Tx whereas the yellow stars are those of the Rx.

We then conduct different training and testing strategies to evaluate the algorithm more practically; the training and testing data are collected separately. In this case, the red and blue lines in Fig. 7 represent the training and testing data, respectively. Specifically, both the training and testing data contain the LOS and NLOS scenarios.

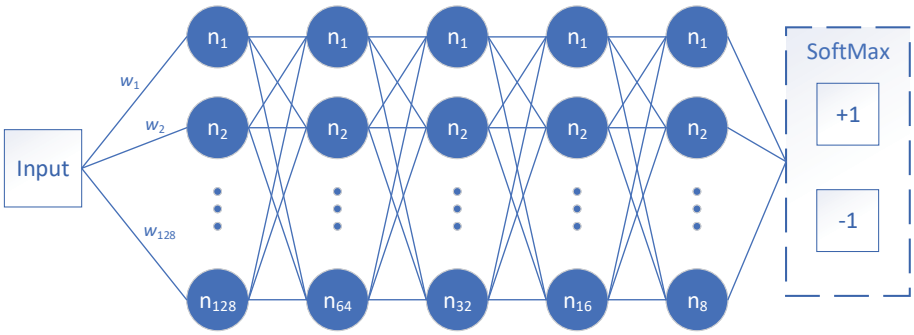

Fig. 5. Illustration of the network architecture.

(a) (b)

(c)

Fig. 6. Antenna arrays and measurement environments. (a) Antenna array on the Tx side. (b) Antenna array on the Rx side. (c) An example of the video shot on the RX side during the measurements.

VI. Evaluation

In this section, we present the evaluation results of the proposed approaches. First, we discuss the database setup, and then elaborate how the selection of different channel features impacts the results. Furthermore, we illustrate and analyze how the the different testing and training strategies affect the results.

A. Database Setup

We apply the V2V measurement data to our proposed LOS identification algorithms. The NLOS situations might arise as moving vehicles, pedestrians, buildings, and other large structures may block the LOS connection. Although the causes of the NLOS condition are the same, the features of the NLOS channels may still be different because the characteristics of the environment where the channel occurs are also different. Noise in the received signal makes the identification even less accurate.

Therefore, we have two categories of evaluation: *i) impact of feature selection* to compare the proposed identification algorithms (we use static and time-varying channel features in this case) with the conventional solutions, and *ii) impact of data selection* to evaluate the different solutions by using different training and testing strategies.

B. Impact of Feature Selection

In the past, researchers used the conventional features, e.g., received power, rising time, and kurtosis, to identify LOS/NLOS channels since their features are usually different [23], [26]. In dynamic V2V channels, each channel feature may contribute differently to the LOS/NLOS identification at a different position along the street.

Fig. 8 gives the probability distribution function (PDF) of the different channel features that were extracted from the measurement data. We can see from the figure that the LOS and NLOS channels indeed show different probability distributions of these features. Most of the features, however,

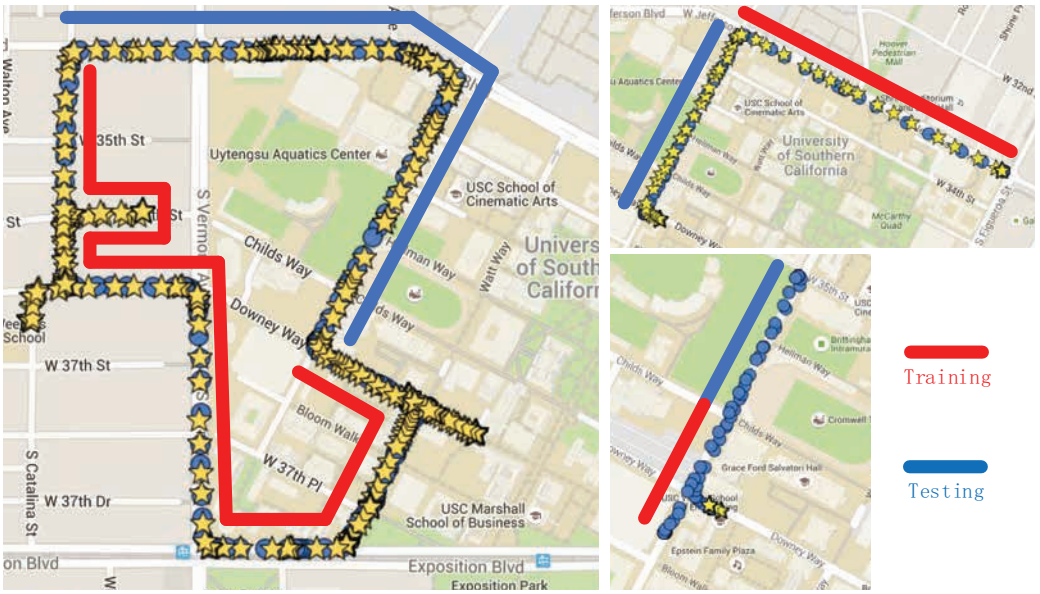

Fig. 7. Illustration of the routes taken during the V2V measurement campaigns. The blue dots and yellow stars represent the positions of the Tx and Rx, respectively. The red and blue lines mark the training and testing data, respectively.

still show some overlapping areas, which may cause the LOS/NLOS to be identified inaccurately, e.g., the solutions in [23] and [26]. Moreover, Figs. 8(g)–(k) show that the angular channel features are more disparate than the other features, and that the PDFs of angular variant features have minimum overlapping area. To evaluate the identification performance more accurately, we conduct a widely used K-fold cross-validation [41]:

1) Each of the databases $\mathbf{X}^{\mathrm{h}}$ and $\mathbf{X}^{\mathrm{l}}$ are divided into K disjoint sets, $\mathbf{X} = \{\mathbf{X}_1 \cup \mathbf{X}_2 \cup \cdots \cup \mathbf{X}_K\}$, with $\mathbf{X}_i \cap \mathbf{X}_j = \emptyset$, for $i \neq j$.
2) We conduct the training based on the set $\mathbf{X} \setminus \mathbf{X}_i$, and then use the set $\mathbf{X}_i$ to validate.
3) We then revalidate the results for each $i = 1, \cdots, K$. In our case, we set $K = 10$ while considering the trade-off between computational complexity and accuracy.

As introduced in the introduction, the most widely used LOS identification method simply uses a fixed threshold of a key parameter of channels, e.g., the Rician K-factor, to classify the measured data. To fully compared to the conventional solutions, we validate the identification performance of using the deterministic threshold of each feature individually. As shown in Fig. 9, the different features indeed show different identification accuracy; both the features of maximum power and angular variant of departure achieve 10% identification error rates; the widely used Rician K-factor doesn't achieve the best performance, probably because the Rician K-factor threshold between LOS and NLOS data may change significantly in the dynamic environment. Note that we use the error rate here to evaluate the identification accuracy, which is calculated by the ratio of the number of incorrectly identified samples over the total number of samples.

To evaluate the effect of selecting different features on the LOS identification, we generate different training sets that consist of different groups of features. Table II shows that each set contains the features tick-marked in the table. The channel features are divided into conventional features and angular-based features; the angular-based features are further divided into static features ($\Delta\lambda_l$, λ_{ASD}, and λ_{ASA}) and temporal features ($\Delta\psi^{\phi_1}$ and $\Delta\psi^{\phi_2}$). We use all the sets in Table II and the PAS data for the training. Thereafter, we implement SVM, RF, and ANN, respectively, for comparison.

Fig. 10 shows the identification error rate of the different classifiers that were generated from the training sets listed in Table II and from the PAS. Specifically, we implement SVM, RF, and ANN for comparison.

Compared to the conventional solutions without machine learning in Fig. 9, it can be found from Fig. 10 that all the machine learning-based solutions are able to achieve better identification accuracy. We can easily see that the selection of training features, as compared to the selection of a machine learning method, has greater effect on identification accuracy. Likewise, we can see in the figure that the RF-based solution mostly outperforms the others in terms of the solutions trained by the extracted features. On the other hand, the ANN has the best performance in the solutions trained by the PAS. This indicates that the RF-based solution is better in identifying the difference between the features extracted from the LOS and NLOS data whereas ANN is better in learning the implicit characteristic from the un-extracted data.

Furthermore, the sets consisting of angular features (sets 2–6) are more accurate than the conventional features (set 1), which are used in [23] and [26], in identifying the LOS/NLOS. This indicates that the angular features have more contribution to the identification process. Specifically, the time-varying angular feature-based solutions (sets 3–6) outperform the static angular feature-based solution (set 2). This indicates that the temporal feature is an important characteristic of the LOS identification in the time-varying system. Set 4 validates the

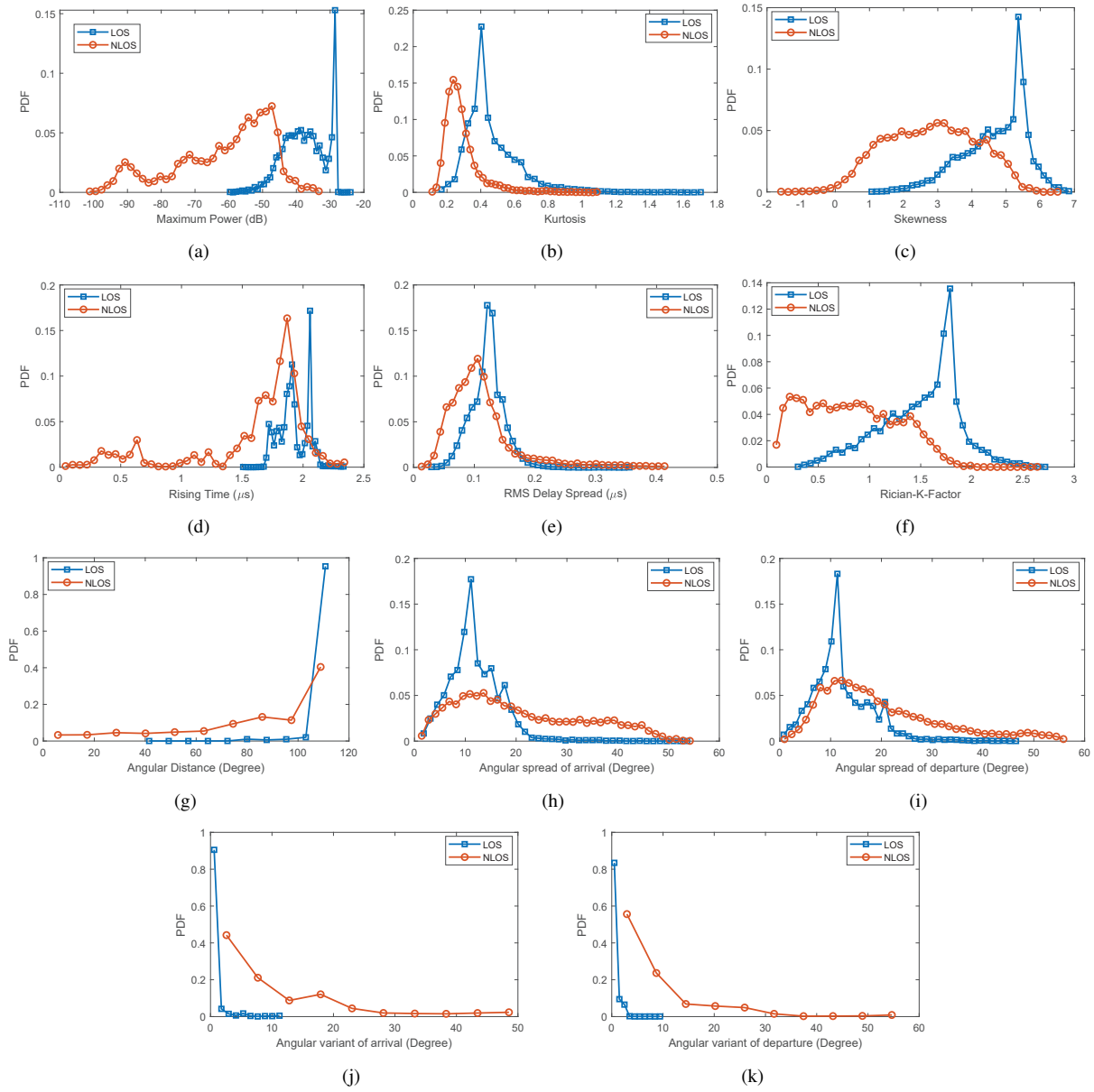

Fig. 8. Probability distribution function of the different extracted characteristics. (a) Maximum power (in dB), (b) Kurtosis, (c) Skewness, (d) Rising time, (e) RMS delay spread, (f) Rician K-factor, (g) Angular distance, (h) AOA, (i) AOD, (j) Angular variant of arrival, and (k) Angular variant of departure.

algorithms trained by using the angular features only; it also shows good accuracy. Moreover, the RF-based solution performs fairly well as trained by the time-varying angular features only.

C. Impact of Data Selection

The validating data in the K-fold cross-validation are iteratively selected from the total data. In practice, however, it is too expensive to measure the channels of all the environments in the city and then label them manually as the training data. Thus, it is more practical to measure some typical scenarios and then generate the classifier for other similar scenarios. We then use different training and testing strategies to do an actual validation of the algorithms as follows:

- Case 1: Conventional K-fold cross validation for training and testing
- Case 2: Different parts of the street for training and testing, respectively
- Case 3: Different streets for training and testing, respectively, as shown in Fig. 7.

Case 1 is the most widely used training strategy for the learning-based classifier [41]. Case 2 is a more practical situation since it requires measuring only a part of each street, although the correlation between the training data and testing data is weaker here than that in case 1. Case 3 is the most practical solution since we only need to measure the typical streets and then validate for all the other streets. In this case, we select the data collected from some streets on campus and some public streets for training. We subsequently validate the algorithms based on the data collected from the totally different streets as shown in Fig. 7. Except for case 1 using K-fold cross-validation, Table III details the validation layout

TABLE II
FEATURE SELECTION FOR DIFFERENT TRAINING SETS

Training set	Channel features										
	Conventional feature						Angular feature				
	Static									Time-varying	
	$\max(\lvert h\rvert^2)$	$\mathcal{K}$	$\mathcal{S}$	$\Delta\tau$	τ_{rms}	K_{r}	$\Delta\lambda_l$	λ_{ASD}	λ_{ASA}	$\Delta\psi^{\phi_1}$	$\Delta\psi^{\phi_2}$
Set 1	√	√	√	√	√	√					
Set 2	√	√	√	√	√	√	√	√	√		
Set 3	√	√	√	√	√	√				√	√
Set 4							√	√	√	√	√
Set 5										√	√
Set 6	√	√	√	√	√	√	√	√	√	√	√

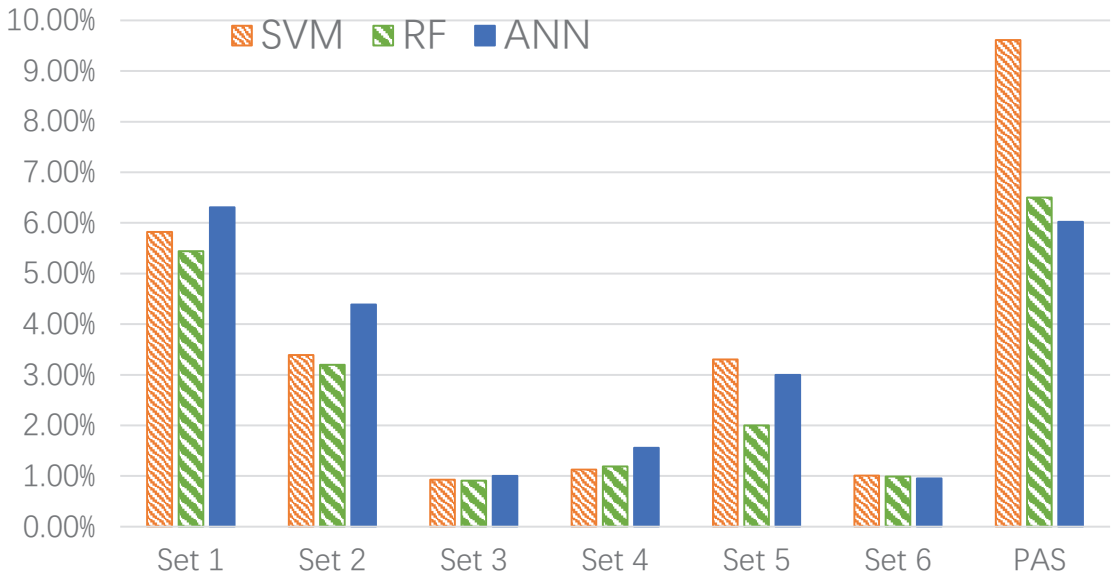

Fig. 10. Identification error rate of the different classifiers that were generated using the training sets listed in Table II and the PAS. Specifically, SVM, RF, and ANN are implemented for comparison.

TABLE III
VALIDATION LAYOUT PARAMETERS

Data sets	Number of data sets
Total LOS/NLOS data sets	1 5295 / 1 3581
Training data for case 2	8 077 / 7 549
Validating data for case 2	7 218 / 6 032
Training data for case 3	7 044 / 5 838
Validating data for case 3	8 251 / 7 743

parameters of cases 2 and 3.

Fig. 11 gives the identification error rate of the different classifiers that were trained using: i) *the conventional features* (set 1), ii) *the angular-based features* (set 6), and iii) *the PAS*. We investigate the impact of data selection on the identification accuracy by comparing the performances of cases 1, 2, and 3. Similarly, we implement SVM, RF, and ANN for comparison.

Similar to the results of the experiments discussed in section VI-B, the selection of training features has the most influence on identification accuracy. Meanwhile, the performance comparison among the different cases shows that all the approaches using case 1 training strategies perform the best whereas the approaches using case 3 have the worst performance. This aspect follows the intuition since the training and validating data in case 3 have the weakest correlation.

We have previously mentioned that both cases 2 and 3 are using totally different data for training and validation. Case 2 still collects training and validating data from the same street whereas case 3 collects them from entirely different streets. In this case, the approaches trained by conventional features show performance differences between cases 2 and 3 that are significantly higher than when trained by angular-based features (both set 6- and PAS-based). This indicates that the angular-based features can improve the robustness of the LOS/NLOS identification even if the validating data change.

Moreover, the ANN-based identification algorithm can still achieve relatively high identification accuracy albeit it is trained only by the PAS. Specifically, in all three cases, the ANN-based solution trained by the PAS performs better

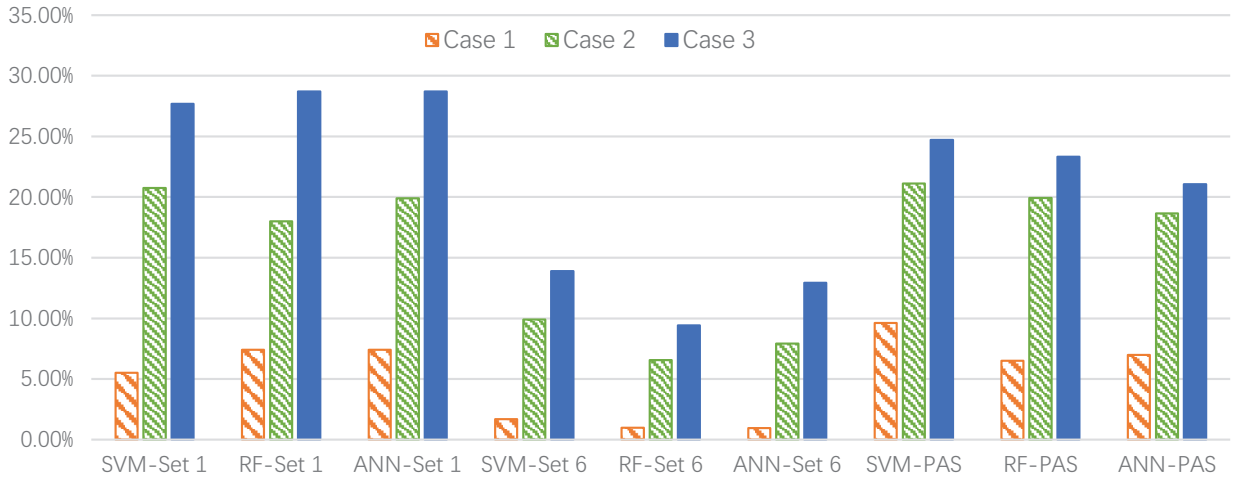

Fig. 11. Identification error rates of the different classifiers that were trained using conventional features (set 1), angular-based features (set 6), and the PAS. The impact of data selection is investigated by comparing the performances of cases 1, 2, and 3. Specifically, SVM, RF, and ANN are implemented for comparison.

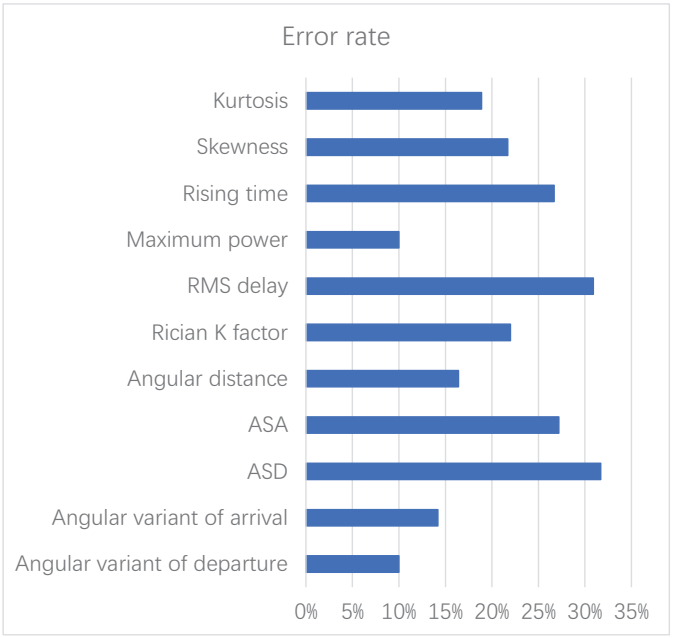

Fig. 9. Identification error rate when deploying the conventional LOS identification solutions, i.e., using a fixed threshold of channel parameters to classify the measured data.

than those trained by conventional extracted features. This is because the PAS data actually contain the un-extracted angular characteristic, which needs to be recognized and can contribute to the identification process. Note that when we compare the performances using the PAS on a dB scale and linear scale for training, the linear scale shows better results. On the other hand, the identification error obtained from using extracted angular characteristics is less than half that obtained from using the PAS, albeit at the price of higher computational complexity.

From the comparison between the approaches using conventional features, i.e., Set 1, it can be found that the SVM-based identification algorithm achieves relatively better performance in both Case 1 and Case 3, whereas the RF-based and ANN-based solutions show similar performance; but the RF-based identification algorithm shows better performance in Case 2 than the other two. Meanwhile, when the angular characteristic is exploited, i.e., Set 2, the RF-based identification algorithm achieves the best performance in all Cases. This indicates that with the help of angular characteristics, the RF algorithm has more robustness than SVM and ANN in the LOS identification problem. Specifically, in the experiment based on PAS set, the RF-based identification even achieves better performance than the ANN-based solution in Case 1, whereas the ANN-based solution still achieves the best performance in the practical cases, i.e., Cases 2 and 3.

The experiment in Fig. 11 shows that the performances of all approaches decrease in a more practical scenario. However, the RF-based approach trained by angular features performs the best whereas the ANN-based approach trained by PAS can provide fairly good accuracy with relatively lower complexity.

In addition, there are several different deep learning methods, e.g., [42]–[45]. Specifically, the convolutional neural network (CNN) shows good performance in feature extraction for channel estimation [43]–[45]. For the training data that consists of spatial features, e.g., the PAS, the CNN may further improve the LOS identification accuracy. To limit the scope of the paper, this work focuses on designing efficient and robust training features for LOS identification and investigating the impact of using different machine learning methods and different training/testing strategies, but further investigation on PAS-based LOS identification by using CNN is an interesting topic for the future.

D. Summary

To sum up, the experiments give us the following conclusions:

- The selection of the training features is the most crucial factor in the performance of LOS identification. This

is confirmed by all the experiments. This gives the intuition that the design of training features should be the major concern for the LOS identification rather than the selection of machine learning methods.

- The angular features can significantly improve the performance of LOS identification. The exploitation of angular characteristics can significantly increase the LOS identification accuracy no matter which other characteristics it is combined with. This observation also follows the insight that the geometry relationship of Tx/Rx and the environment has a strong connection with the LOS/NLOS propagation process.
- The ANN can well recognize the implicit characteristic of the PAS and can identify the LOS/NLOS conditions with fair accuracy while using a relatively lower computational complexity. Unlike the extracted channel characteristics, the PAS contains the channel features that are submerged in "noise information", i.e., cannot be directly used for LOS identification. Benefitting from feature mining, the ANN can automatically extract the features that contribute to LOS identification, and thus achieves the best performance when the method is only trained by PAS. Considering the time-consuming channel feature extraction process, the ANN-based identification trained by PAS can be an alternative and fast solution for LOS identification.
- The RF-based LOS/NLOS identification gives the best performance based on the extracted training features. It can be found from all the experiments, the RF-based identification shows better robustness, especially when the training features contains the angular channel characteristic. This may because the RF method is better in-learning the artificial-extracted channel feature, i.e., the angular channel characteristic, compared with SVM and ANN in our case.
- Most of the solutions perform worse when totally different training and validating data are used. However, the angular features can improve the robustness of the LOS/NLOS identification to this effect. From the comparison among the three cases we conducted, the angular channel features are able to narrow the gap of identification performance in different cases.

VII. Conclusion

In this paper, we have proposed two novel algorithms to address the problem of LOS identification. They are based on channel features extracted from measured MIMO impulse responses either through HRPE or low-resolution (Fourier) estimation. According to the evaluations based on extensive V2V measurement data, the algorithms can accurately and effectively identify LOS/NLOS conditions. Furthermore, we have compared the impact of the selection of training methods, i.e., SVM, RF, ANN, on the identification accuracy. The RF shows the best performance as trained by the extracted temporal features. On the other hand, the ANN achieves the best identification accuracy as trained by the PAS data. In addition, we have evaluated the algorithms by using different training and validating strategies. The proposed algorithms show good robustness to environmental changes, indicating that application without exhaustive training data acquisition drives might be feasible. All experiments are conducted by using the fullyconnected layer-based network structure, a more accurate ANN structure will be investigated in future work.

References

[1] R. M. Vaghefi and R. M. Buehrer, "Cooperative joint synchronization and localization in wireless sensor networks," *IEEE Trans. Signal Process.*, vol. 63, no. 14, pp. 3615–3627, Jul. 2015.

[2] T. Lu, H. Gao, X. Li, S. Yang, and L. Hanzo, "Space-time hierarchical-graph based cooperative localization in wireless sensor networks," *IEEE Trans. Signal Process.*, vol. 64, no. 2, pp. 322–334, Jan. 2016.

[3] Y. Shen and M. Z. Win, "On the accuracy of localization systems using wideband antenna arrays," *IEEE Trans. Commun.*, vol. 58, no. 1, pp. 270–280, Jan. 2010.

[4] S. Gezici *et al.*, "Localization via ultra-wideband radios: A look at positioning aspects for future sensor networks," *IEEE Signal Process. Mag.*, vol. 22, no. 4, pp. 70–84, Jul. 2005.

[5] R. Casas, A. Marco, J. J. Guerrero, and J. Falco, "Robust estimator for non-line-of-sight error mitigation in indoor localization," *EURASIP J. Appl. Signal Process.*, vol. 2006, pp. 156–156, Jan. 2006.

[6] B. Denis and N. Daniele, "NLOS ranging error mitigation in a distributed positioning algorithm for indoor UWB ad-hoc networks," in *Proc. Int. Wksh. Wirel. ADHOC-NOW*, Oulu, 2004, pp. 356–360.

[7] C. Huang, A. F. Molisch, R. Wang, P. Tang, R. He, and Z. Zhong , "Machine-learning-based data processing techniques for vehicle-to-vehicle channel modeling," *IEEE Commun. Mag.*, vol. 57, no. 11, pp. 109–115, November 2019.

[8] 3GPP TSG RAN, "Spatial channel model for multiple input multiple output (MIMO) simulations," 3GPP, Tech. Rep., pp. 1–41, 2004.

[9] L. Liu *et al*., "The COST 2100 MIMO channel model," *IEEE Wirel. Commun.*, vol. 19, no. 6, pp. 92–99, Dec. 2012.

[10] F. Jameel, Z. Hamid, F. Jabeen, S. Zeadally,and M. A. Javed, "A survey of device-to-device communications: Research issues and challenges," *IEEE Commun. Surveys Tut.*, vol. 20, no. 3, pp. 2133–2168, Apr. 2018.

[11] R. I. Ansari *et al.*, "5G D2D networks: Techniques, challenges, and future prospects," *IEEE Syst. J.*, vol. 12, no. 4, pp. 3970–3984, Dec. 2018.

[12] Y. Yuan, C. Wang, Y. He, M. M. Alwakeel, and E. M. Aggoune, "3D wideband non-stationary geometry-based stochastic models for non-isotropic MIMO vehicle-to-vehicle channels," *IEEE Trans. Wirel. Commun.*, vol. 14, no. 12, pp. 6883–6895, Dec. 2015.

[13] X. Cai, B. Peng, X. Yin, and A. P. Yuste, "Hough-transform-based cluster identification and modeling for V2V channels based on measurements," *IEEE Trans. Veh. Technol.*, vol. 67, no. 5, pp. 3838–3852, May 2018.

[14] R. He, B. Ai, G. L. Stuber, G. Wang, and Z. Zhong, "Geometrical-based modeling for millimeter wave MIMO mobile-to-mobile channels," *IEEE Trans. Veh. Technol.*, vol. 67, no. 4, pp. 2848–2863, Apr. 2018.

[15] R. He *et al.*, "Vehicle-to-vehicle radio channel characterization in crossroad scenarios," *IEEE Trans. Veh. Technol.*, vol. 65, no. 8, pp. 5850–5861, Aug. 2016.

[16] R. Wang, O. Renaudin, C. U. Bas, S. Sangodoyin, and A. F. Molisch, "Vehicle-to-vehicle propagation channel for truck-to-truck and mixed passenger freight convoy," In *Proc. 2017 IEEE 28th Annu. Int. Symp. PIMRC*, Montreal, QC, 2017, pp. 1–5.

[17] P. Tang, J. Zhang, A. F. Molisch, P. Smith, M. Shafi, and L. Tian, "Estimation of the *K*-factor for temporal fading from single-snapshot wideband measurements," *IEEE Trans. Veh. Technol.*, vol. 68, no. 1, pp. 49–63, Oct. 2018.

[18] S. Marano, W. M. Gifford, H. Wymeersch, and M. Z. Win, "NLOS identification and mitigation for localization based on UWB experimental data," *IEEE IEEE J. Sel. Areas Commun.*, vol. 28, no. 7, pp. 1026–1035, Sept. 2010.

[19] Z. Xiao, H. Wen, A. Markham, N. Trigoni, P. Blunsom and J. Frolik, "Non-line-of-sight identification and mitigation using received signal strength," *IEEE Trans. Wirel. Commun.*, vol. 14, no. 3, pp. 1689–1702, March 2015.

[20] Z. Xiao, H. Wen, A. Markham, N. Trigoni, P. Blunsom and J. Frolik, "Identification and mitigation of non-line-of-sight conditions using received signal strength," in *Proc. 2013 IEEE 9th International Conference on Wireless and Mobile Computing, Networking and Communications (WiMob)*, Lyon, 2013, pp. 667–674.

[21] T. Van Nguyen, Y. Jeong, H. Shin, and M. Z. Win, "Machine learning for wideband localization," *IEEE J. Sel. Areas Commun.*, vol. 33, no. 7, pp. 1357–1380, Jul. 2015.

[22] E. Kurniawan, L. Zhiwei, and S. Sun, "Machine learning-based channel classification and its application to IEEE 802.11ad communications," in *Proc. 2017 IEEE GLOBECOM*, Singapore, 2017, pp. 1–6.

[23] F. Xiao, Z. Guo, H. Zhu, X. Xie, and R. Wang, "AmpN: Real-time LOS/NLOS identification with WiFi," in *Proc. 2017 IEEE ICC*, Paris, 2017, pp. 1–7.

[24] A. Decurninge *et al.*, "CSI-based outdoor localization for massive MIMO: Experiments with a learning approach," in *Proc. 15th ISWCS*, Lisbon, 2018, pp. 1–6.

[25] C. Huang, A. F. Molisch, R. Wang, P. Tang, R. He, and Z. Zhong , "Angular information-based NLOS/LOS identification for vehicle to vehicle MIMO system," in *Proc. 2019 IEEE International Conference on Communications Workshops (ICC Workshops)*, Shanghai, China, 2019, pp. 1–6.

[26] K. Gururaj, A. K. Rajendra, Y. Song, C. L. Law, and G. Cai, "Real-time identification of NLOS range measurements for enhanced UWB localization," in *Proc. 2017 Int. Conf. IPIN*, Sapporo, 2017, pp. 1–7.

[27] P. Almers *et al.*, "Survey of channel and radio propagation models for wireless MIMO systems," *EURASIP J. Wirel. Commun. Netw.*, vol. 2007, Dec. 2007.

[28] B. H. Fleury, M. Tschudin, R. Heddergott, D. Dahlhaus, and K. I. Pedersen, "Channel parameter estimation in mobile radio environments using the SAGE algorithm," *IEEE J. Sel. Areas Commun.*, vol. 17, no. 3, pp. 434–450, Mar. 1999.

[29] A. Richter, "Estimation of radio channel parameters: Models and algorithms," PhD dissertation, Technischen Universitat Ilmenau, Ilmenau, Germany, Dec. 2005.

[30] B. H. Fleury, "First- and second-order characterization of direction dispersion and space selectivity in the radio channel," *IEEE Trans. Inf. Theory*, vol. 46, no. 6, pp. 2027–2044, Sept. 2000.

[31] C. Huang *et al*., "A power-angle-spectrum based clustering and tracking algorithm for time-Varying radio channels," *IEEE Trans. Veh. Technol.*, vol. 68, no. 1, pp. 291–305, Jan. 2019.

[32] M. S. Bartlett, "Smoothing periodograms from time-series with continuous spectra," *Nature*, vol. 161, no. 4096, pp. 686–687, May 1948.

[33] C. Cortes and V. Vapnik, "Support-vector networks," *Mach. Learn.*, vol. 20, no. 3, pp. 273–297, Sept. 1995.

[34] J. A. K. Suykens and J. Vandewalle, "Least squares support vector machine classifiers," *Neural Process. Lett.*, vol. 9, no. 3, pp. 293–300, Jun. 1999.

[35] M. Buhmann, *Radial Basis Functions: Theory and Implementations*, 1st ed. Cambridge, U.K.: Cambridge Univ. Press, 2003.

[36] L. Breiman, "Random Forest," *Mach. Learn.*, vol. 45, no. 1, pp. 5–32, Oct. 2001.

[37] L. Breiman, J. Friedman., R. Olshen, and C. Stone, *Classification and Regression Trees*. Belmont, CA: Wadsworth, 1984.

[38] R. Lippmann, "An introduction to computing with neural nets," *IEEE ASSP Mag.*, vol. 4, no. 2, pp. 4–22, Apr. 1987.

[39] R. Wang, C. U. Bas, O. Renaudin, S. Sangodoyin, U. T. Virk, and A. F. Molisch, "A real-time MIMO channel sounder for vehicle-to-vehicle propagation channel at 5.9 GHz," in *Proc. 2017 IEEE ICC*, Paris, 2017, pp. 1–6.

[40] R. Wang, O. Renaudin, C. U. Bas, S. Sangodoyin, and A. F. Molisch, "High-resolution parameter estimation for time-varying double directional V2V channel," *IEEE Trans. Wirel. Commun.*, vol. 16, no. 11, pp. 7264–7275, Nov. 2017.

[41] C. E. Rasmussen and C. K. I. Williams, *Gaussian Processes for Machine Learning*. Berlin: Springer, 2006.

[42] H. He, C. Wen, S. Jin, and G. Y. Li, "Model-driven deep learning for joint MIMO channel estimation and signal detection," arXiv:1907.09439, 2019.

[43] H. Huang, J. Yang, H. Huang, Y. Song and G. Gui, "Deep learning for super-resolution channel estimation and DOA estimation based massive MIMO system," *IEEE Trans. Veh. Technol.*, vol. 67, no. 9, pp. 8549–8560, Sept. 2018.

[44] Y. Wang, M. Liu, J. Yang and G. Gui, "Data-driven deep learning for automatic modulation recognition in cognitive radios," *IEEE Trans. Veh. Technol.*, vol. 68, no. 4, pp. 4074–4077, April 2019.

[45] G. Gui, H. Huang, Y. Song and H. Sari, "Deep learning for an effective nonorthogonal multiple access scheme," *IEEE Trans. Veh. Technol.*, vol. 67, no. 9, pp. 8440–8450, Sept. 2018.

Chen Huang (S'17) received the B.E. and M.S. degrees from Chongqing University of post and telecommunications (CQUPT), Chongqing, China, in 2013 and 2016, respectively. He is currently pursuing the Ph.D. degree with the School of Computer and Information Technology, Beijing Jiaotong University (BJTU), Beijing, China. From 2018 to 2019, he has been a Visiting Scholar with the University of Southern California, Los Angeles, CA, USA. He is currently a visiting scholar at the Université Catholique de Louvain (UCL), Louvain-la-Neuve, Belgium.

Mr. Chen received two times the Best Paper Award at international conferences, and serves as the Technical Program Committee (TPC) member for VTC-full 2019. His research interests include channel parameters analysis and characterization, clustering and tracking for time-varying channel modeling, and applications of machine learning-based techniques on propagation channel characterization.

Andreas F. Molisch (S'89M'95SM'00F'05) received the Dipl. Ing., Ph.D., and habilitation degrees from the Technical University of Vienna, Vienna, Austria, in 1990, 1994, and 1999, respectively. He subsequently was with FTW (Austria), AT&T (Bell) Laboratories Research (USA); Lund University, Sweden, and Mitsubishi Electric Research Labs (USA). He is now a Professor and the Solomon Golomb Andrew and Erna Viterbi Chair at the University of Southern California, Los Angeles, CA, USA.

His current research interests are the measurement and modeling of mobile radio channels, multi-antenna systems, wireless video distribution, ultra-wideband communications and localization, and novel modulation formats. He has authored, coauthored, or edited four books (among them the textbook Wireless Communications, Wiley-IEEE Press), 20 book chapters, more than 250 journal papers, more than 340 conference papers, as well as more than 80 patents and 70 standards contributions.

Dr. Molisch has been an Editor of a number of journals and special issues, General Chair, Technical Program Committee Chair, or Symposium Chair of multiple international conferences, as well as Chairman of various international standardization groups. He is a Fellow of the National Academy of Inventors, Fellow of the AAAS, Fellow of the IET, an IEEE Distinguished Lecturer, and a Member of the Austrian Academy of Sciences. He has received numerous awards, among them the Donald Fink Prize of the IEEE, the IET Achievement Medal, the Armstrong Achievement Award of the IEEE Communications Society, and the Eric Sumner Award of the IEEE.

Ruisi He (S'11-M'13-SM'17) received the B.E. and Ph.D. degrees from Beijing Jiaotong University (BJTU), Beijing, China, in 2009 and 2015, respectively.

Since 2015, Dr. He has been with the State Key Laboratory of Rail Traffic Control and Safety, BJTU, where he has been a Full Professor since 2018. Dr. He has been a Visiting Scholar in Georgia Institute of Technology, USA, University of Southern California, USA, and Université Catholique de Louvain, Belgium. His research interests include measurements and modeling of wireless channels, machine learning and clustering analysis in communications, vehicular and high-speed railway communications, 5G massive MIMO and high frequency communication techniques. He has authored/co-authored 4 books, 2 book chapters, more than 100 journal and conference papers, as well as several patents.

Dr. He is an Editor of the IEEE Transactions on Wireless Communications, the IEEE Antennas and Propagation Magazine, the IEEE Communications Letters, and a Lead Guest Editor of the IEEE Journal on Selected Area in Communications. He serves as the Early Career Representative (ECR) of Commission C, International Union of Radio Science (URSI). He received the IEEE ComSoc Asia-Pacific Outstanding Young Researcher Award in 2019, the URSI Young Scientist Award in 2015, and five Best Paper Awards in conferences. He is a member of the COST.

Rui Wang received the B.S. degree from Southeast University, Nanjing, China in 2010. He received the M.S. degree (Hons.) in 2012, and the Doctorate degree in Electrical Engineering in 2018 from the University of Southern California, Los Angeles, CA, USA. He is currently a research engineer at Samsung Research America. His research interests include wireless channel measurements and modeling for vehicle-to-vehicle and mm-wave communication systems. He is also interested in statistical signal processing and optimization algorithms.

Pan Tang received the B.S. degree in Electrical Information Engineering from the South China University of Technology, Guangzhou, China, in 2013 and the Ph.D. degree in Information and Communication Engineering from the Beijing University of Posts and Telecommunications, Beijing, China, in 2019. In 2017, he was a Visiting Scholar with the University of Southern California. Now, he is a Postdoctoral Researcher in the State Key Laboratory of Networking and Switching Technology, Beijing University of Posts and Telecommunications, China. His current research interests include millimetre-wave, THz, and V2V channel measurements and modelling.

Bo Ai (M00SM10) received the M.S. and Ph.D. degrees from Xidian University, Xian, China, in 2002 and 2004, respectively.

He was with Tsinghua University, Beijing, China, where he was an Excellent Postdoctoral Research Fellow in 2007. He is currently a Professor with Beijing Jiaotong University, where he is also the Deputy Director of the State Key Laboratory of Rail Traffic Control and Safety. He is also currently with the Engineering College, Armed Police Force, Xian. He has authored or coauthored six books and 230 scientific research papers and holds 26 invention patents in his research areas. His interests include the research and applications of orthogonal frequency-division multiplexing techniques, high-power amplifier linearization techniques, radio propagation and channel modeling, global systems for mobile communications for railway systems, and long-term evolution for railway systems.

Dr. Ai is a Fellow of the Institution of Engineering and Technology. He has been a Co-chair or a Session/Track Chair for many international conferences, such as the ninth International Heavy Haul Conference in 2009; the 2011 IEEE International Conference on Intelligent Rail Transportation; HSRCom2011; the 2012 IEEE International Symposium on Consumer Electronics; the 2013 International Conference on Wireless, Mobile, and Multimedia; the 2013 IEEE Green HetNet; and the IEEE 78th Vehicular Technology Conference in 2014. He is an Associate Editor of IEEE TRANSACTIONS ON CONSUMER ELECTRONICS and an Editorial Committee Member of the Wireless Personal Communications journal. He has received many awards, such as the Qiushi Outstanding Youth Award from the HongKong Qiushi Foundation, the New Century Talents from the Chinese Ministry of Education, the Zhan Tianyou Railway Science and Technology Award from the Chinese Ministry of Railways, and the Science and Technology New Star from the Beijing Municipal Science and Technology Commission.

Zhangdui Zhong (SM'16) received the B.E. and M.S. degrees from Beijing Jiaotong University, Beijing, China, in 1983 and 1988, respectively.

He is currently a Professor and an Advisor of Ph.D. candidates with Beijing Jiaotong University, where he is also currently a Chief Scientist of State Key Laboratory of Rail Traffic Control and Safety. He is also the Director of the Innovative Research Team of Ministry of Education, Beijing, and a Chief Scientist of Ministry of Railways, Beijing. He is an Executive Council Member of the Radio Association of China, Beijing, and a Deputy Director of the Radio Association, Beijing. His interests include wireless communications for railways, control theory and techniques for railways, and GSM-R systems. His research has been widely used in railway engineering, such as the Qinghai-Xizang railway, Datong-Qinhuangdao Heavy Haul railway, and many high-speed railway lines in China. He has authored or coauthored seven books, five invention patents, and more than 200 scientific research papers in his research area.

Prof. Zhong received the Mao YiSheng Scientific Award of China, Zhan TianYou Railway Honorary Award of China, and Top 10 Science/Technology Achievements Award of Chinese Universities.